Supporting Information

Soft Elastomers with Programmable Stiffness as Strain-Isolating Substrates for Stretchable Electronics

Min Cai[‡], Shuang Nie[‡], Yipu Du[‡], Chengjun Wang, Jizhou Song*

Department of Engineering Mechanics, Soft Matter Research Center, and Key Laboratory of Soft Machines and Smart Devices of Zhejiang Province, Zhejiang University, 310027 Hangzhou, China

[‡]*These authors contributed equally to this work.*

[*]*To whom correspondence should be addressed. jzsong@zju.edu.cn*

Supplementary note 1: Finite element analysis

Three-dimensional (3D) finite element models were established to simulate the mechanical behaviors of strain-isolating substrates with or without devices on it under uniaxial stretches in ABAQUS. The thickness of the strain-isolating substrate is 145 μm. The elastic moduli of HMR (8 mm long and 8 mm wide) and LMR (16 mm long and 8 mm wide) are 2.76 MPa and 0.12 MPa, respectively. The Poisson's ratio is set as 0.48 for both HMR and LMR. The modulus and Poisson's ratio of the homogeneous substrate is 1.0 MPa and 0.48, respectively. The elastic modulus and Poisson's ratio of gold film (4 mm long, 3 mm wide and 100 nm thick) are 70 GPa and 0.44, respectively. The ultrathin temperature sensor element (TSE) and stretchable organic photodiode (OPD) are modeled as a three-layer composite consisting of the bottom PI supporting layer (6 μm thick), middle gold layer (80 nm thick), and the PI encapsulation layer (4 μm thick). The Young's modulus and Poisson's ratio of PI are 2.5 GPa and 0.34, respectively. The shell element (S4) is used to discretize the gold film, TSE and OPD. The 8-node linear brick element (C3D8R) is used to discretize the substrate. To ensure the convergence of finite element analysis, the smallest element size is set as 2 μm, which is below 1/4 of the minimum characteristic device length.
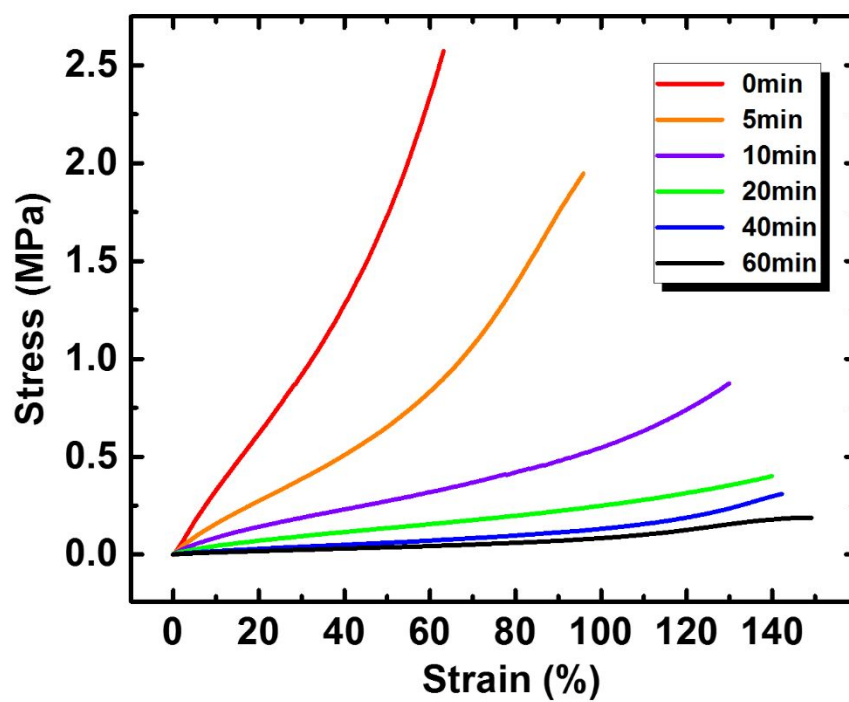
Figure S1. The stress-strain curves for the BP-PDMS substrate samples with various UV exposure time.
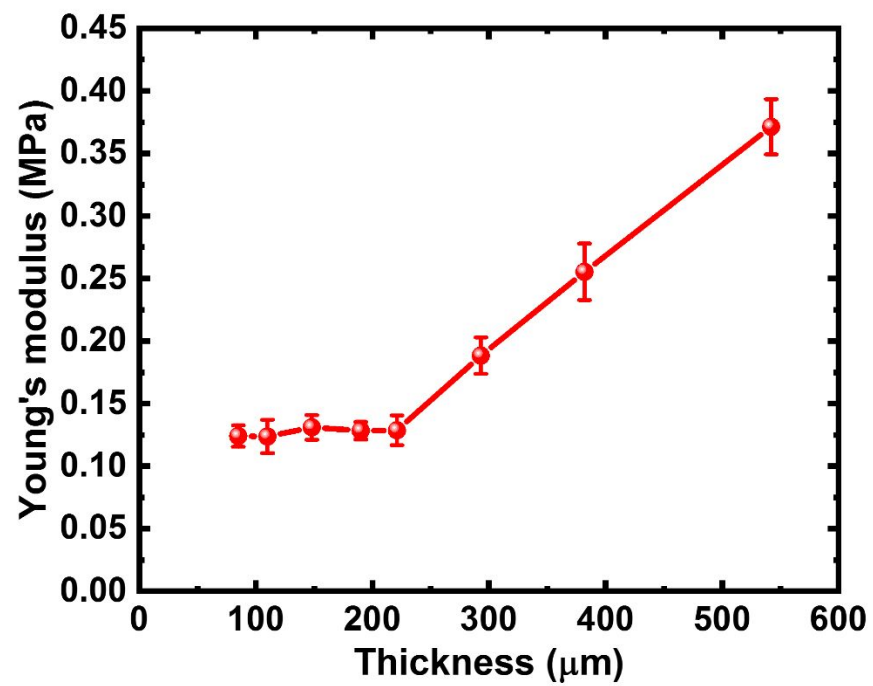
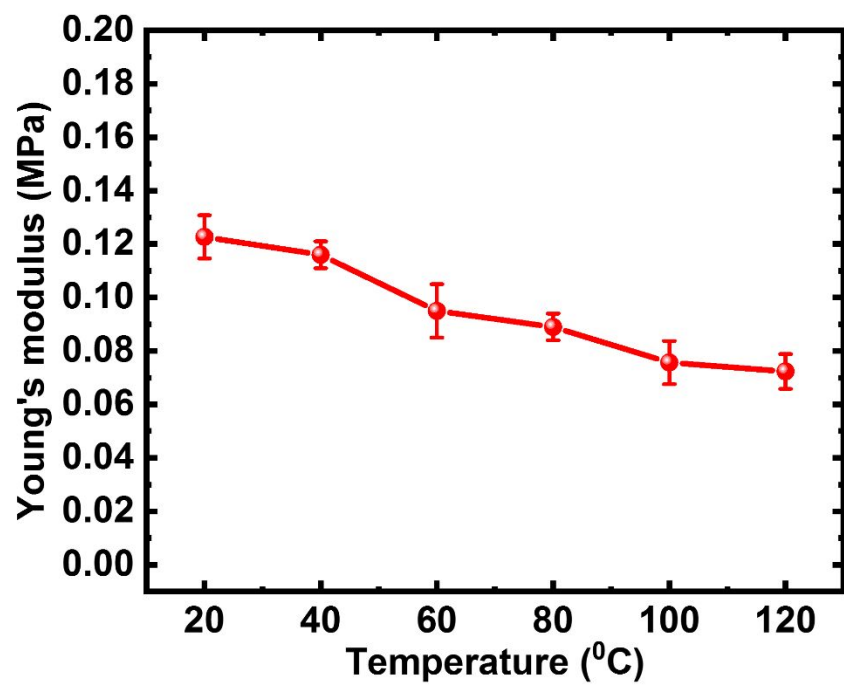**Figure S2.** The influence of the BP-PDMS thickness on the Young's modulus.

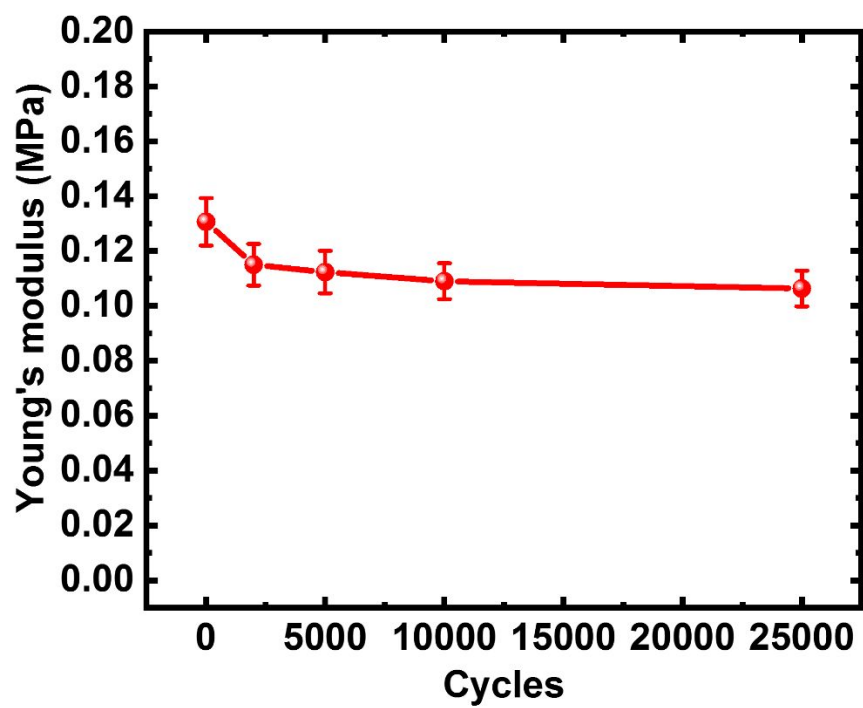**Figure S3.** The dependence of the Young's modulus of BP-PDMS on the temperature.

Figure S4. The Young's modulus of BP-PDMS versus cycles under the stretch of 50%.
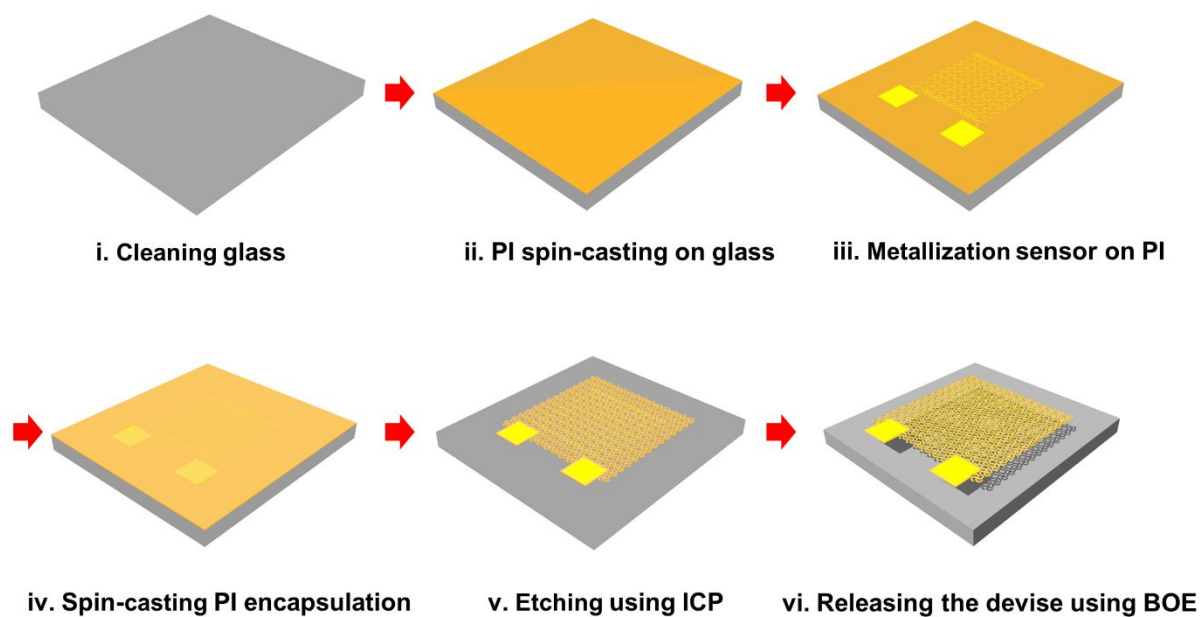
i. Cleaning glass   **ii. PI spin-casting on glass**   **iii. Metallization sensor on PI**

iv. Spin-casting PI encapsulation   **v. Etching using ICP**   **vi. Releasing the devise using BOE**

Figure S5. The fabrication process of the TSE.

a

mesh

PI traces

300 μm | 285x | 15kV -Mapping | OCT 03 2018 19:24
948 μm | BSD Topo B | streched

b

bonding pad with
Au exposed

300 μm | 280x | 15kV -Mapping | OCT 03 2018 19:30
955 μm | BSD Topo B | streched

c

Au embedded in PI
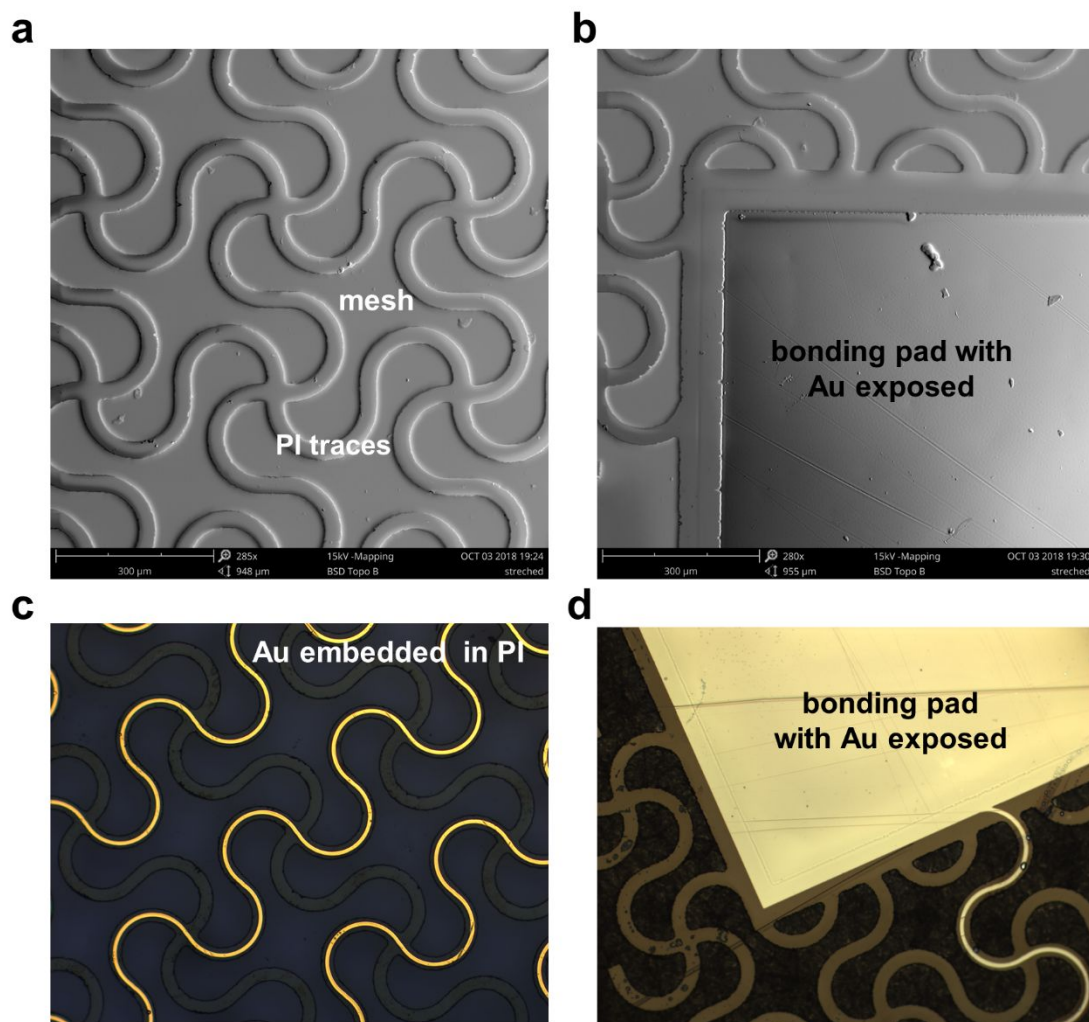
d

bonding pad
with Au exposed

Figure S6. The open mesh layout of TSE. (a) SEM image of the serpentine PI traces. (b) SEM image of the bonding pad. (c) Optical image of the serpentine PI traces. (d) Optical image of the bonding pad.
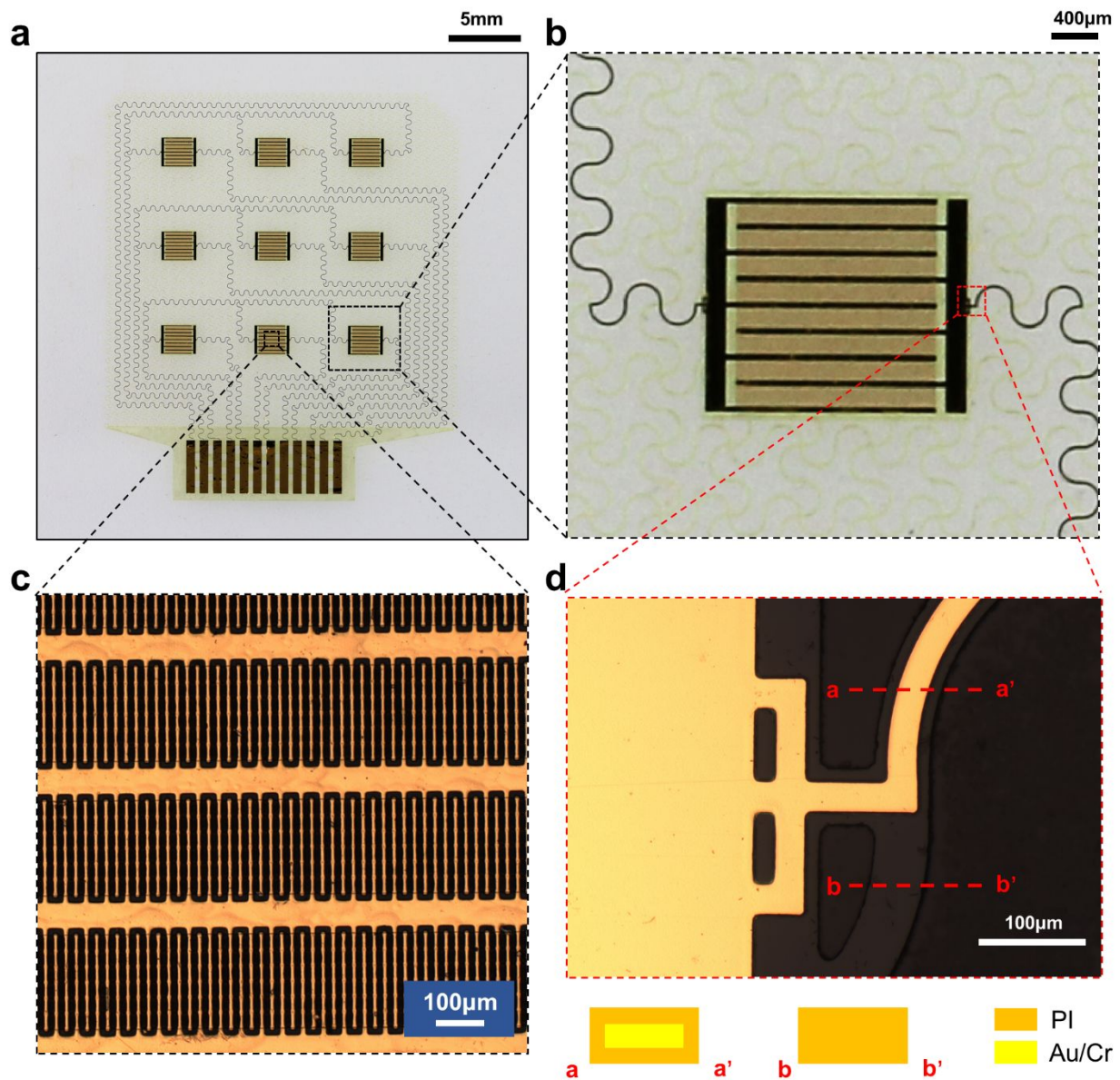
Figure S7. (a) Optical image of IDE array. (b-d) Magnified views of the IDE in different sections.
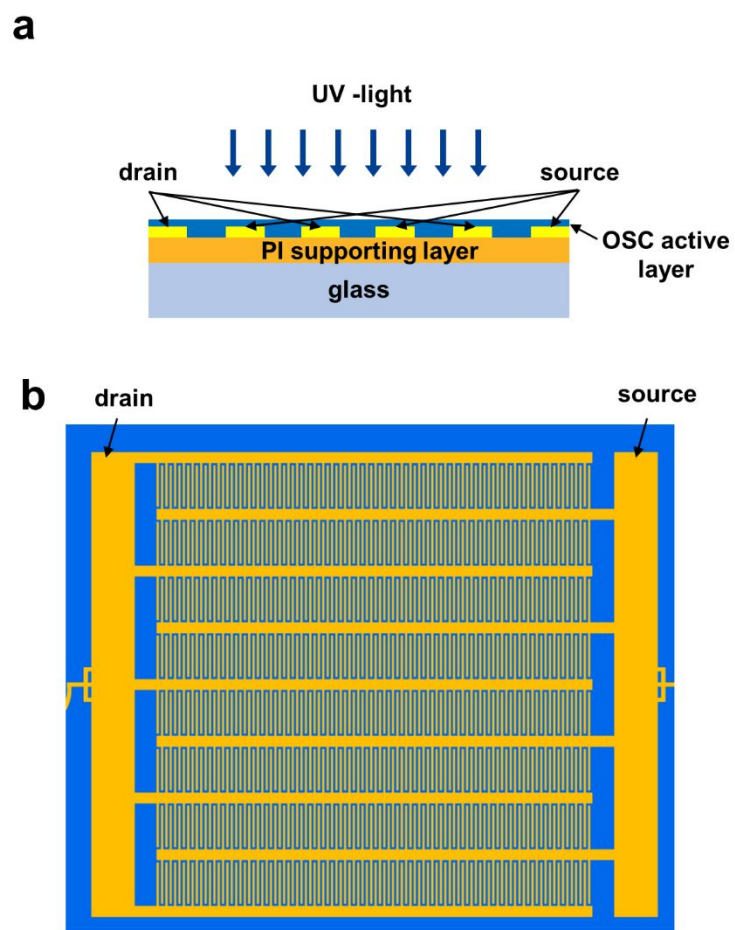
a

UV -light

drain   source

PI supporting layer   OSC active layer

glass

b   drain   source

Figure S8. Schematic illustration of the structure of the OPD. (a) Cross-sectional view. (b) Top view.
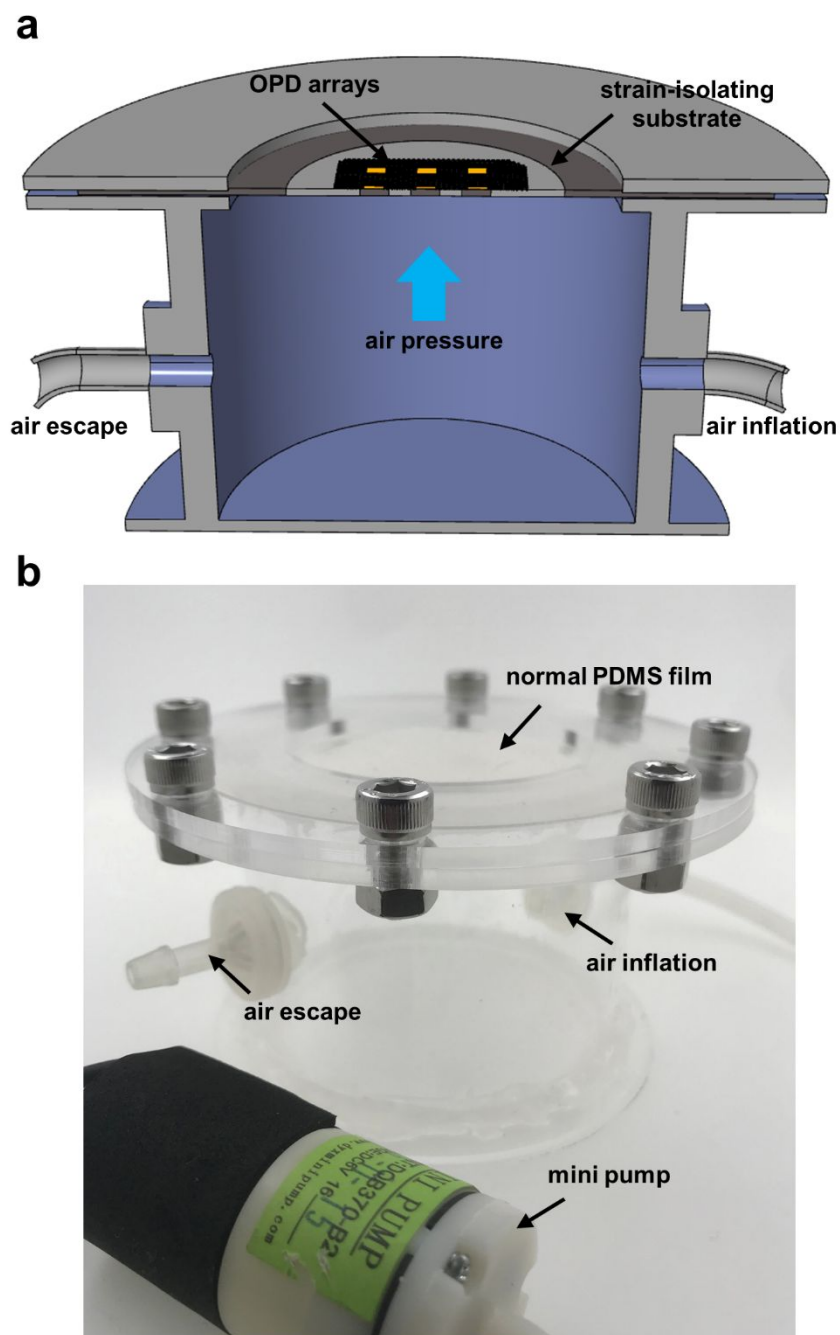
Figure S9. (a) Schematic illustration of the cross-sectional view of the pressure-tunable cylindrical cavity. (b) Optical image of the pressure-tunable cylindrical cavity connected with a mini pump.
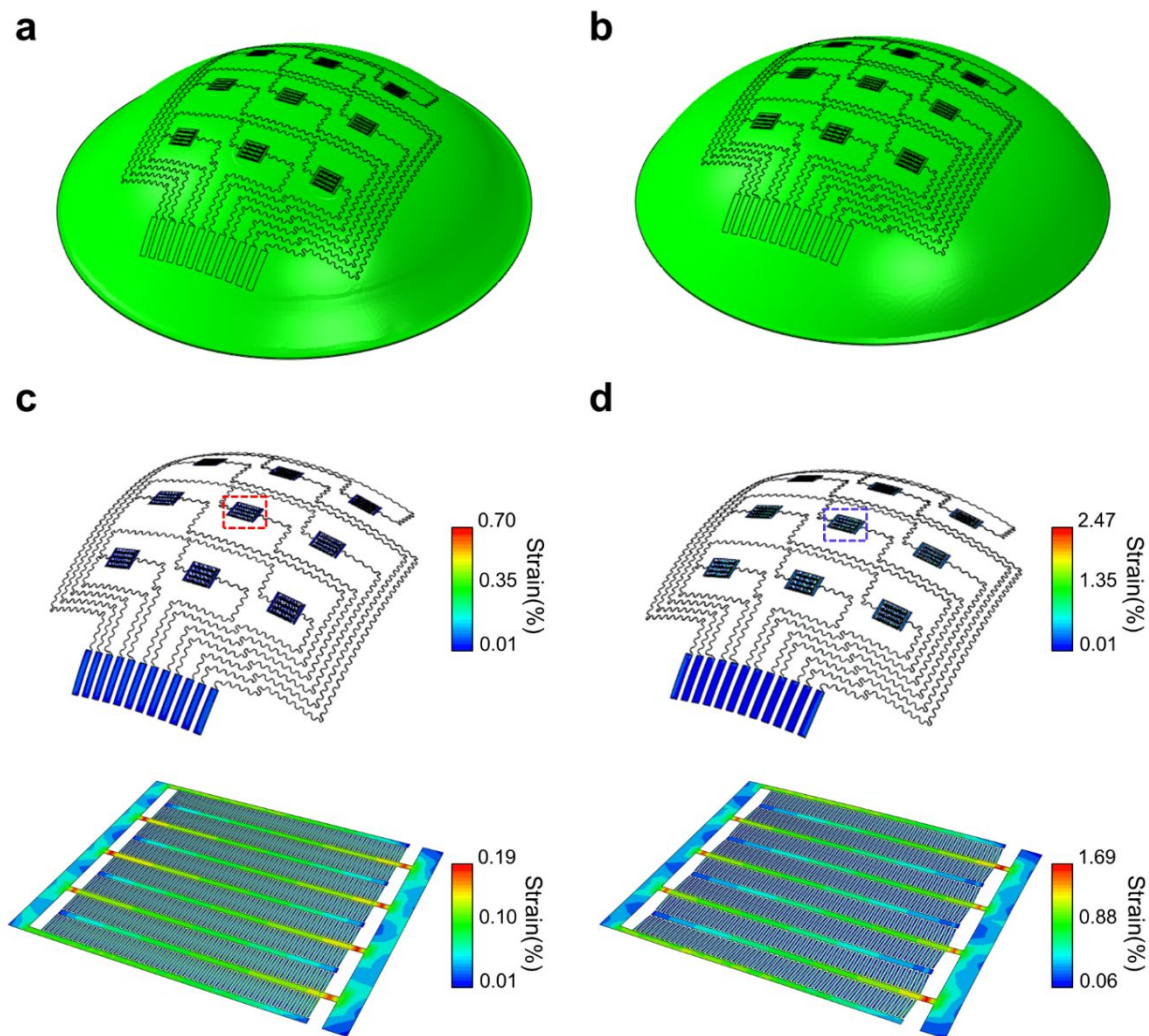
Figure S10. (a,b) The deformed configurations of the OPD array w/ and w/o strain isolation. (c,d) The maximum principal strain distributions in the metal layers w/ and w/o strain isolation, highlighting the maximum principal strain distributions in the OPD element.